ICARUS 68, 217–238 (1986)

The Spatial Distribution of Rocks on Mars

PHILIP R. CHRISTENSEN

Department of Geology, Arizona State University, Tempe, Arizona 85287

Received April 9, 1986; revised June 16, 1986

The spatial distribution of rocks exposed at the surface of Mars has been mapped using Viking Infrared Thermal Mapper (IRTM) observations. Overall, there are no regions on the surface of Mars at a scale of 1° × 1° in latitude and longitude that are rock free. The modal value of rock abundance is 6% areal coverage, with no areas having more than 30–35% rock cover. The model developed to determine rock abundance relates the thermal emission in each of the four surface-sensing IRTM bands to temperature contrasts within the field of view, non-unit thermal emissivity due to absorption bands in the surface materials, and the absorption and scattering of the outgoing energy by atmospheric dust and water ice. Each of these effects produce characteristic spectral and diurnal signatures, allowing them to be separated. The temperature contrasts provide a means to determine both the abundance of exposed rocks and the fine-component thermal inertia. Rock abundance alone does not produce the observed variation in bulk thermal inertia of the surface. Low-inertia (fine), bright surfaces have fewer rocks exposed than do high-inertia (coarse), dark surfaces. Rock abundance does not correlate well with the RMS slope nor reflectivity determined from delay-Doppler radar measurements. There is, however, a possible correlation between RMS slope determined from continuous-wave radar observations. Dual-polarization radar measurements, which provide the best radar measure of small-scale roughness, indicate that the Tharsis volcanic region is very rough, whereas thermal measurements indicate very few rocks and a covering of dust. Together these observations suggest an approximately 1-m-thick mantle of fines covering a very rough subsurface. This fine material may be an aeolian deposit of dust storm fallout. Valles Marineris, together with several major channels and chaotic terrains, have high rock abundances, as does the Acidalia Planitia basin. This observed distribution may reflect the initial deposition of coarse material associated with channel formation. Syrtis Major is unique in having a high inertia but a very low rock abundance, together with low radar roughness. These observations are consistent with mantling of rocks by sand. The observed distribution of rocks and fines indicates that aeolian processes, both erosional and depositional, play a dominant role in shaping the present Martian surface.

I. INTRODUCTION

An important goal in the study of Mars is to understand the geologic history and evolution of the surface. The present surface has been shaped by volcanic, aeolian, fluvial, glacial, periglacial, and cratering processes, all of which can erode, deposit, and transport the surface materials. Because this complex variety of processes cannot be observed *in situ* over geologic time, their activity must be inferred by studying the small-scale surface characteristics they produce. Of particular importance is the particle size distribution, including fines and rocks, which provides a strong constraint on the degree of erosion and deposition that has occurred. The purpose of this paper is to discuss the use of Viking Infrared Thermal Mapper (IRTM) observations to determine the surface rock abundance on Mars. These data will be compared to other morphological and remote-sensing information to provide a basis for discussing the age and degree of modification which has occurred. In addition, these results will be compared to previous surface roughness estimates, both as a test of the relative accuracy of the different methods, and to study possible wavelength-dependent differences in roughness measurements which provide additional constraints on the size and degree of burial of the surface rocks.

Several remotely determined measure-

0019-1035/86 $3.00

ments have been used to determine surface properties. These include: visible reflectance observations to determine the albedo and microscale roughness (Thorpe, 1977, 1982; Pleskot and Miner, 1981); radar measurements of millimeter-to-meter roughness and large-scale surface undulations (e.g., Downs *et al.*, 1975; Simpson *et al.*, 1978a, b, 1984; Harmon *et al.*, 1982); passive microwave measurements to study the surface and subsurface structure (Cuzzi and Muhleman, 1972; Jakosky and Muhleman, 1980); and thermal observations to determine the bulk thermophysical properties of the surface (Kieffer *et al.*, 1977; Jakosky, 1979; Palluconi and Kieffer, 1981; Christensen, 1986; Jakosky and Christensen, 1986a,b).

In addition to determining the average thermal inertia and grain size of the surface, thermal observations can also be used to separate the surface emission into a rock and fine component (Christensen, 1982). This technique is based on the kinetic temperature contrast that exists between fine surface materials and the exposed rocks, with rocks being cooler during the day and warmer at night than the surrounding fines. This mixture of nonuniform temperatures results in a non-Planck distribution of emitted energy. Using observations of the surface emission at more than one wavelength, the energy distribution can be inverted and the temperature and abundance of two components can be determined. Two additional, complicating effects are the emission and scattering of energy by atmospheric dust and clouds and the non-unit thermal emissivity of the surface, both of which also produce a non-Planck distribution of emitted energy. These three effects can be modeled and separated to provide maps of surface rock abundance, thermal emissivity, and an estimate of the atmospheric dust content. A preliminary model was developed and used to determine the rock abundance for six regions on Mars (Christensen, 1982). A description of the model and its application to surface properties and processes is presented in the following sections.

II. ROCK ABUNDANCE MODEL

The IRTM instrument provided observations in four surface-sensing bands centered on 7, 9, 11, and 20 μm (Kieffer *et al.*, 1977). At each wavelength the emitted energy was converted to brightness temperature (e.g., T_{20}) using the Planck function and assuming unit emissivity. Real variations from a blackbody cause these brightness temperatures to differ between wavelengths, producing non-zero spectral differences (e.g., T_7–T_{20}). The entire surface of Mars was observed at multiple times of day and at all seasons, with a typical surface resolution of 30 km. It is this suite of multiple observations that allows the numerous variables that contribute to the observed spectral differences to be separated. Each of the major contributing factors—rocks, thermal emissivity, and atmospheric dust—have very unique diurnal signatures as shown in Fig. 1. Using diurnal observations, each parameter of the model can be varied until a unique fit to the data is made (Fig. 2; Christensen, 1982). This method is time consuming, however, and is not suited to global mapping of rock abundance. Once the general character of the surface has been determined and the time of day at which the model is most sensitive to surface rocks, the model can, however, be automated to determine the rock abundance from single observations.

The effects of atmospheric dust can be minimized or eliminated by restricting the time of day of the observations used to be between 0 and 5H, and by using observations acquired during the clearest periods (Fig. 1; Christensen, 1982). A quantitative estimate of the contribution by dust indicates that less than 10% of the observed spectral differences are due to dust during these time periods (Zurek, 1982), based on estimates of the dust optical properties determined from Mariner 9 IRIS observations

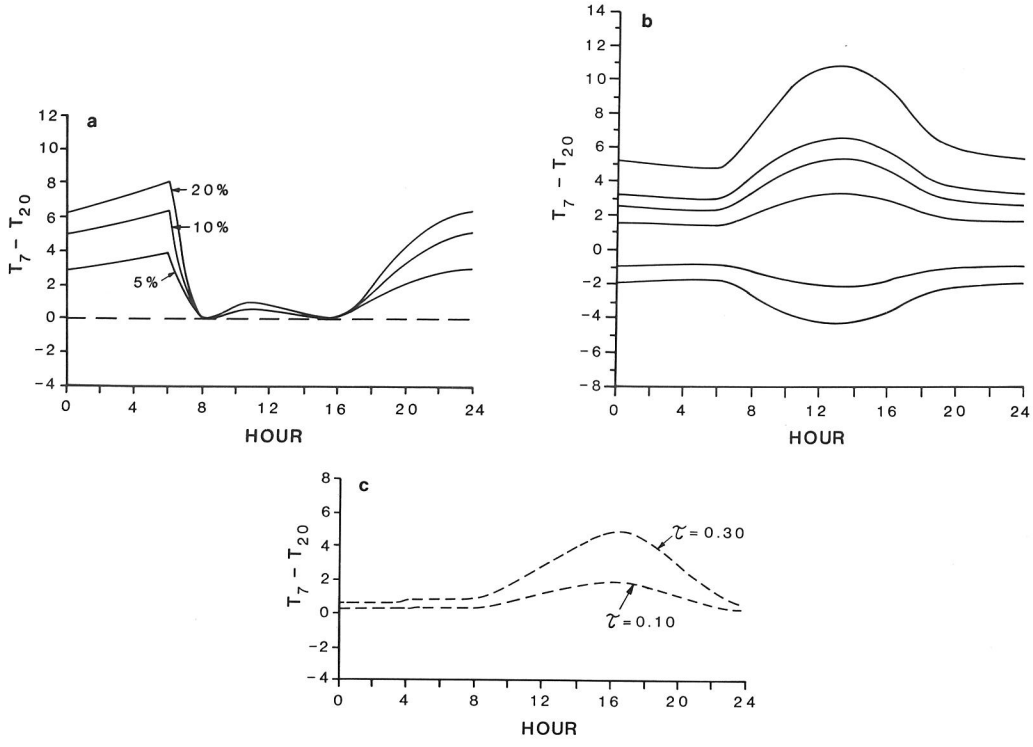

FIG. 1. Diurnal variation of T_7–T_{20}. The basic model was run for latitude = 0°, L_s = 100°, a fine-component inertia and albedo of 4 and 0.25, respectively, and a rock inertia of 30°. (a) Effect of rocks. (b) Effect of thermal emissivity. Emissivity values for each curve are from top to bottom: (1) $C_7 = 1.0$, $C_{20} = 0.9$; (2) $C_7 = 0.9$, $C_{20} = 0.9$; (3) $C_7 = 1.0$, $C_{20} = 0.95$; (4) $C_7 = 0.95$, $C_{20} = 0.95$; (5) $C_7 = 0.95$, $C_{20} = 1.0$; (6) $C_7 = 0.9$, $C_{20} = 1.0$. (c) Effect of atmospheric dust.

(Toon *et al.*, 1977), the dust opacity (Pollack *et al.*, 1979; Pleskot and Miner, 1981), and the atmospheric temperature profile (Conrath *et al.*, 1973; Seiff and Kirk, 1977).

Non-unit surface emissivity can produce a significant contribution to the spectral differences (Christensen, 1982). The magnitude of this effect is directly proportional to surface temperature and can thus be minimized by again restricting the time of day of observations used to be from 0 to 5*H*. Preliminary studies of the variation of surface emissivity showed a strong correlation with surface albedo, with low-albedo regions having emissivities varying from 0.92 at 20 μm to 0.97 at 7 μm and high-albedo regions having emissivities of near-unity at all wavelengths (Christensen, 1982). More detailed studies using data acquired during the time period when the effects of rocks and atmospheric dust are minimized (7.5–9.5*H* and 14.5–16.5*H*) have confirmed these general trends but have revealed subtle variations in emissivity for a given albedo

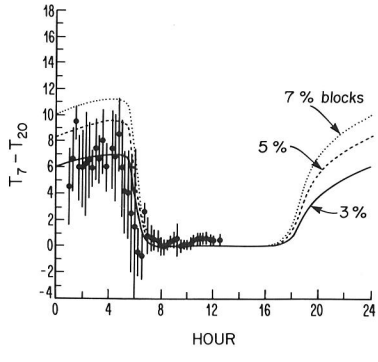

FIG. 2. Fit of model to T_7–T_{20} Arabia data. Data from the Arabia region (26 to 34°N, 318 to 338°W) are shown, compared to models using 3, 5, and 7% surface rock abundance.

(Christensen, 1984). However, these differences do not produce significant changes in the derived rock abundances. In the results discussed here, rock abundances were computed for each of two cases: (1) with no correction for emissivity, and (2) with the contribution from emissivity found for the global correlation with albedo removed. A comparison of these results will be discussed below.

To determine the abundance of surface rocks, a numerical model was developed that has as parameters the thermal inertia, emissivity, and albedo of the fine and rock components. Although the Martian surface has a range of rock sizes (Mutch *et al.*, 1977; Binder *et al.*, 1977), the model developed here was limited to two components to provide a realistic model, yet one with a limited number of free parameters.

The kinetic temperature of each component (i) was determined from

$$T_i = T_m + (\partial T/\partial A)(A_i - A_m) + (\partial T/\partial I)(I_i - I_m)F(I_i) \quad (1)$$

where T_m is a base model temperature for albedo A_m and inertia I_m (given in units of 10^{-3} cal cm^{-2} sec$^{-1/2}$ °K^{-1}), I_i and A_i are the inertia and albedo of each component, $\partial T/\partial I$ and $\partial T/\partial A$ are partial derivatives of temperature with albedo and inertia, respectively, and $F(I)$ corrects for the nonlinearity of T with I (Christensen, 1983). This temperature model is described in detail in Kieffer *et al.* (1977); the diurnal variation of $\partial T/\partial A$ and $\partial T/\partial I$ is given in Kieffer *et al.* (1973).

The kinetic temperature of the rocks and fines was used to determine the emitted flux ($B(T)$) using the Planck function and the appropriate emissivity (ε) as a function of wavelength (λ). The net flux ($F(\lambda)$) as a function of wavelength was computed by summing the two components, multiplied by the fraction of the surface covered by each, as given by

$$F(\lambda) = \alpha\varepsilon_r(\lambda)B(T_r) + (1 - \alpha)\varepsilon_f(\lambda)B(T_f) \quad (2)$$

where subscript r refers to rock and f to fines, and α is the fraction of the surface covered by rocks.

The computed values for $F(\lambda)$ were convolved with the IRTM instrument response function to generate a brightness temperature in each IRTM band. These brightness temperatures can be differenced and compared to observed spectral differences for the Martian surface. The free parameters in the model are the rock abundance (α), and the inertia, albedo, and emissivity of the rock and fine components. An initial estimate of the inertia and albedo was chosen using the values for each point found by Palluconi and Kieffer (1981) and Pleskot and Miner (1981), respectively. Previous work demonstrated that the rock abundances are generally less than 25% and are lower in low-inertia regions (Christensen, 1982). For these conditions the fine component inertia is a weak function of rock abundance, and is generally within 1 of the effective inertia of the composite surface determined by Palluconi and Kieffer (1981).

Using this model, brightness temperatures were generated for each IRTM band, which were than compared to the observed values and tested for convergence. Once the rock abundance was determined an effective inertia for the composite surface was computed and compared to the composite value. If these values differed by more than 1, the fine-component inertia was adjusted and the computation repeated. The process was repeated in an iterative fashion by varying α and the inertia of the fine component using Newton's method and the partial derivatives of spectral difference with rock fraction and inertia to solve for rock abundance. For each point, two rock abundances were determined, one with and one without an emissivity correction.

The sensitivity of the rock abundance determination in this model is a direct function of the kinetic temperature contrast between the rocks and fines, which is controlled by the thermophysical proper-

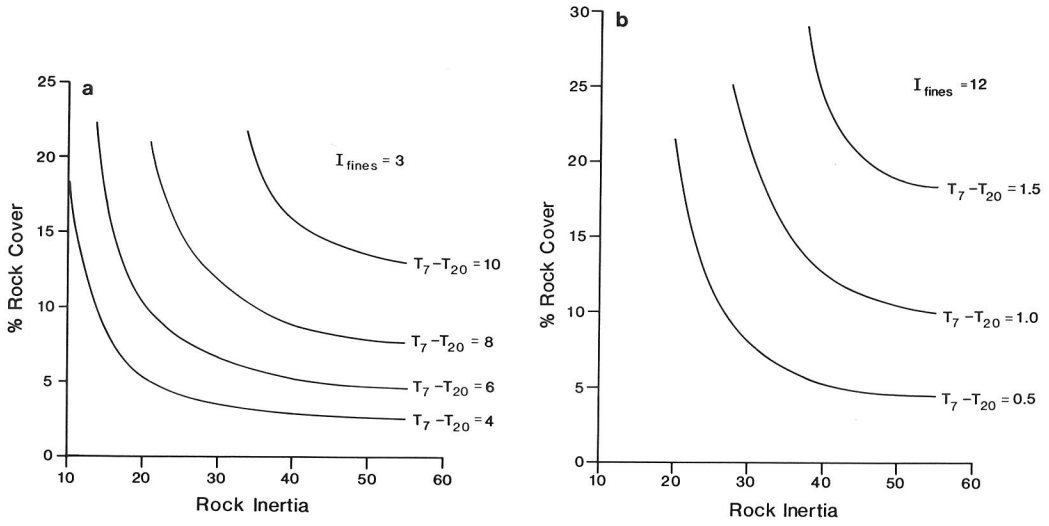

FIG. 3. Variation of rock abundance with rock inertia. The latitude for these models was 0°, L_s was 100°, and local hour was $3H$. Three separate values for observed T_7–T_{20} are shown for illustration. (a) Fine-component inertia of 3; (b) fine-component inertia of 12.

ties of the rocks and fines. To determine the temperature of the rocks, the inertia and albedo of the rock component were fixed at 30 and 0.1, respectively, and the emissivities were taken to be those for the darkest material found on the Martian surface (Christensen, 1982). This choice of inertia corresponds to rocks approximately 15 cm in diameter (Christensen, 1982). As the radius of the rock approaches the diurnal skin depth for solid rock (~15 cm), further increases in rock size will not alter the temperature of the rock. Therefore, rocks larger than approximately 30 cm will have an effective inertia of ~55. Rocks smaller than 15 cm will have lower effective inertias, with values approaching a limiting value of 10 for unconsolidated particles larger than 1 mm (Jakosky, 1986). Figure 3 illustrates the effect of varying rock inertia on the computed rock abundance. For these models, the L_s was 100°, latitude was 0°, the local hour was $3H$ ($24H$ equals one Martian day), the rock albedo was 0.1, and the albedo of the fines was 0.25. Two different fine-component inertias of 3 and 12 were used. For a fixed, observed value of T_7–T_{20}, the rock abundance determined from the model increases as the rock inertia decreases (Fig. 3). For rock inertias greater than 30 (rock diameter > 15 cm), the change in abundance is typically less than 40%. For rocks smaller than 15 cm, the derived rock abundance can increase by up to 100%.

Assuming a fixed rock inertia of 30, the sensitivity is determined by the inertia of the fine component. Figure 4 shows the variation in the T_7–T_{20} spectral difference as a function of fine-component inertia for 5, 10, and 20% rock cover. The absolute uncertainty in brightness temperature is less than 0.2°K for each IRTM band (Kieffer *et al.*, 1977) resulting in an uncertainty in the difference of less than 0.4°K.

In summary, the model described here provides estimates of rock abundance once the contributing effects of emissivity and atmospheric dust are removed. Atmospheric dust produces uncertainties in rock abundance of less than 10% of the derived value. Uncertainties due to emissivity depend on both the absolute value of emissivity and the accuracy to which emissivity is

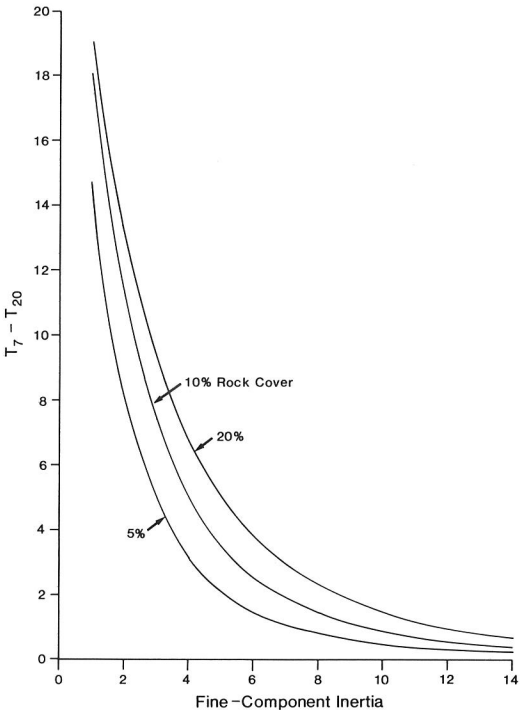

FIG. 4. Variation of T_7–T_{20} with fine-component inertia and rock abundance. Time of day for these models was $3H$, latitude was 0°, L_s was 100°.

known. For emissivities close to 1.0 (bright regions), the uncertainty in emissivity is approximately 10%; for emissivities close to 0.9, as found for the darkest regions, the uncertainty is up to 20%. Because the correction for an emissivity of 0.9 lowers the rock abundance by up to 60%, the resulting error in derived rock abundance is 15% of the value determined. Actual values of rock inertia other than that assumed would result in values up to 30% lower if the rocks were larger than 10 cm or a factor of 2 higher if the rocks were much smaller. Finally, the sensitivity of the rock determination is a strong function of the fine-component inertia, with rock abundance determined to within ±1% for low-inertia regions, and ±5% for high-inertia regions. Overall, then, the absolute abundance of rocks is accurate to within a factor of 2. As will be seen, this uncertainty does not affect the conclusions reached.

The absolute value of the fine-component inertia is much less sensitive to uncertainties in the properties assumed for the rock component. The factor of 2 uncertainty in rock abundance produces an uncertainty of less than 0.5 in the fine-component inertia.

III. RESULTS

Observations

The data used to determine surface rock abundances were obtained by the Viking Orbiter (VO) 1 IRTM instrument on orbits 786 to 845 (Aug. 22 to Oct. 27, 1978; aerocentric longitude (L_s) 132° to 166°) and by VO2 on orbits 459 to 536 (Oct. 26, 1977 to March 23, 1978; L_s 355° to 63°). These periods were chosen to minimize the atmospheric dust content, which contributes to the observed spectral signature and complicates the analysis of surface properties. The data were also constrained to be between 0 and $5H$ to further reduce the effects of atmospheric dust and surface emissivity. Within these time periods a uniform set of predawn observations with surface resolutions of 30 to 50 km was made by each spacecraft as their orbits precessed around the planet. Rock abundances were derived using the VO1 and VO2 T_7–T_{20}, T_9–T_{20}, and T_{11}–T_{20} data. The rock abundances were computed separately for each observation, and then collected into 1° × 1° bins in latitude and longitude to reduce the uncertainty of the observations.

Rock Abundance

The rock abundances determined for each set of observations were compared to test for consistency. In some areas there were major differences in rock abundance determined using the T_{11} and T_7 data. These differences are primarily due to the presence of significant water-ice absorption within the 11-μm band, which increases the T_{11}–T_{20} spectral contrast at night and appears as a higher rock abundance. Water-ice clouds are consistently observed in the northern hemisphere from 60° to 240° W

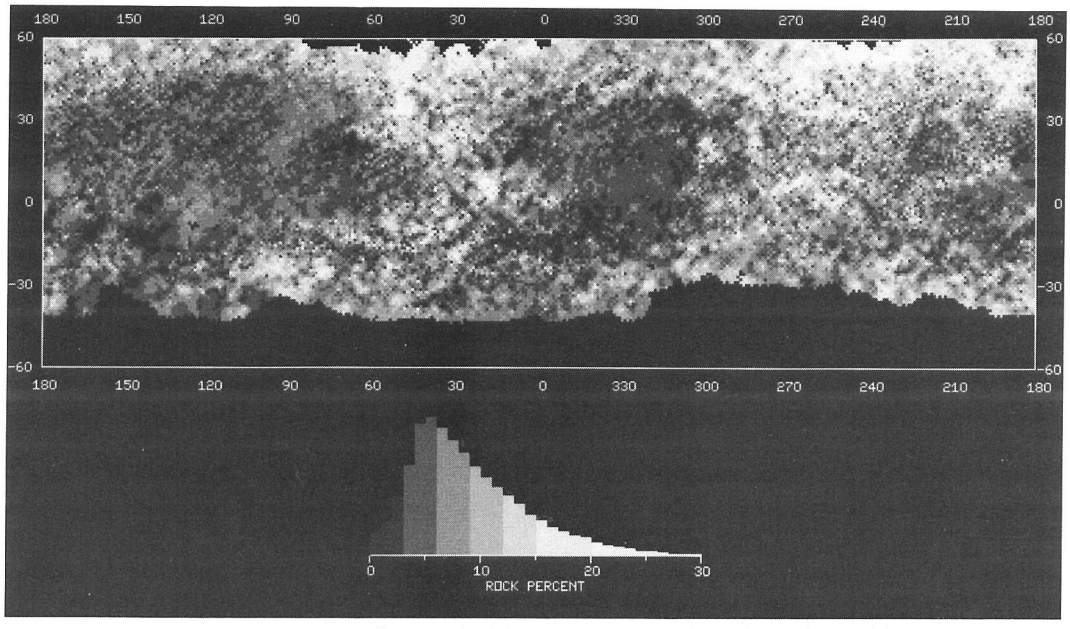

FIG. 5. Rock abundance. Combined map using VO1 T_7–T_{20} data from 60°N to −30°S. VO2 data were used to extend coverage south of −30°S.

and 310° to 30° W longitude (Christensen and Zurek, 1984; Christensen *et al.*, 1986). These locations agree very well with the regions observed to have higher apparent rock abundance in the T_{11}–T_{20} data compared to the T_7–T_{20} observations. The occurrence of water-ice clouds varies seasonally and diurnally, and is therefore difficult to model and remove from global observations. For this reason, the T_{11}–T_{20} data were not used to determine global rock abundances.

Rock abundances computed using the T_9–T_{20} data were consistently higher than those found using T_{11}–T_{20} or T_7–T_{20}, a finding previously noted from the diurnal observations (Christensen, 1982). This difference is most likely due to the presence of atmospheric dust. Although the dust load was the lowest during the period observed here (Pleskot and Miner, 1981; Martin, 1986), some dust is always present in the atmosphere (Pollack *et al.*, 1979). Radiative transfer calculations using the particle size distribution and composition estimated from Mariner 9 IRIS observations (Toon *et al.*, 1977) indicate that dust produces a factor of 4 larger difference in T_9–T_{20} than in T_{11}–T_{20} or T_7–T_{20} (Christensen, 1982; R. Zurek, private communication). Because of the possible contamination by atmospheric dust, the T_9–T_{20} data are also not considered to provide a good estimate of the surface rock abundance.

The VO1 and VO2 T_7–T_{20} data, corrected for non-unit emissivity, do provide a useful measure of surface rock abundance, and have been used to construct a global map of rock abundance, given in Fig. 5. For bright, low-inertia surfaces the rock abundances are nearly equal with and without a emissivity correction, as expected because the emissivity of these regions is close to unity. However, within regions where the albedos are the lowest, such as Acidalia Planitia (10–50°N, 0–60°W) and Syrtis Major (0–30°N, 290–310°W) the global emissivity corrections do produce significant changes in the rock abundance. In some cases, these corrections overcompensate for the ob-

TABLE I

Area	Lat. range	Long. range	Albedo	Single point *with* emissivity correction		Single point *no* emissivity correction		Diurnal fit	
				Mean	σ	Mean	σ	Mean	σ
Arabia	26–34°N	318–338°	0.27	5.6	1.8	6.1	1.8	5	2
Isidis	8–12°N	266–278°	0.23	10.3	5.1	17.5	4.9	10	5
Syrtis Major	2–14°	286–296°	0.11	6.4	3.3	15.9	3.0	10	5
Acidalia Planitia	30–40°N	20– 45°	0.15	12.7	4.4	26.1	4.6	15	5
Viking 1 Lander site	20–24°N	45– 50°	0.25	13.7	4.0	18.7	2.8	15	5
Viking 2 Lander site	46–50°N	224–228°	0.26	17.1	2.5	18.5	1.7	20	10

served spectral differences. These regions therefore contain the greatest uncertainty in rock abundance. However, with or without an emissivity correction, these areas have among the highest rock abundances observed.

The histograms of rock abundance for all of the cases studied are unimodal, except for the VO1 T_{11}–T_{20} data which were contaminated by the presence of water-ice clouds. As discussed previously, the rock determinations are uncertain by up to a factor of 2. This uncertainty is not systematic, however, and should not affect the overall distribution of rocks observed. The T_7–T_{20} data, corrected for emissivity, have a modal value of 6% (Fig. 5). The minimum rock abundance found for all cases was 1%, with no regions observed to have no rocks exposed at the surface. The maximum values found remain near 25% in all cases. This value probably represents an upper limit on the fraction of rocks exposed on Mars at a scale of 1° × 1°. For exposed bedrock with an inertia of 55, the maximum areal extent is 12%.

As a means of evaluating the model developed here, the rock abundances with and without an emissivity correction have been averaged for six regions whose rock abundance was previously determined by fitting models to diurnal observations (Christensen, 1982). The locations of these regions and the results from the two techniques are given in Table I. Comparison of the values shows that the rock abundances computed for bright regions agree very well between the two methods, and there is little difference between values with and without an emissivity correction. In dark regions, where the emissivities are lowest, the abundances decrease significantly after the correction is made for emissivity. This correction brings the computed rock abundances into good agreement with the values found by fitting the diurnal observations where emissivity was a free parameter. From this comparison, it appears that the model described here reproduces the results determined from the more complete modeling using diurnal observations, provided that a correction is made to remove the contributions due to non-unit emissivity.

Fine-Component Thermal Inertia

As discussed previously, the fine-component inertia is a free parameter in these models, whose value is adjusted to provide a fit to the average inertia of the composite surface. The thermal inertia of the fine-component surface materials corresponding to the rock abundances given in Fig. 5 is shown in Fig. 6. For comparison, the effective inertia of the surface, derived from di-

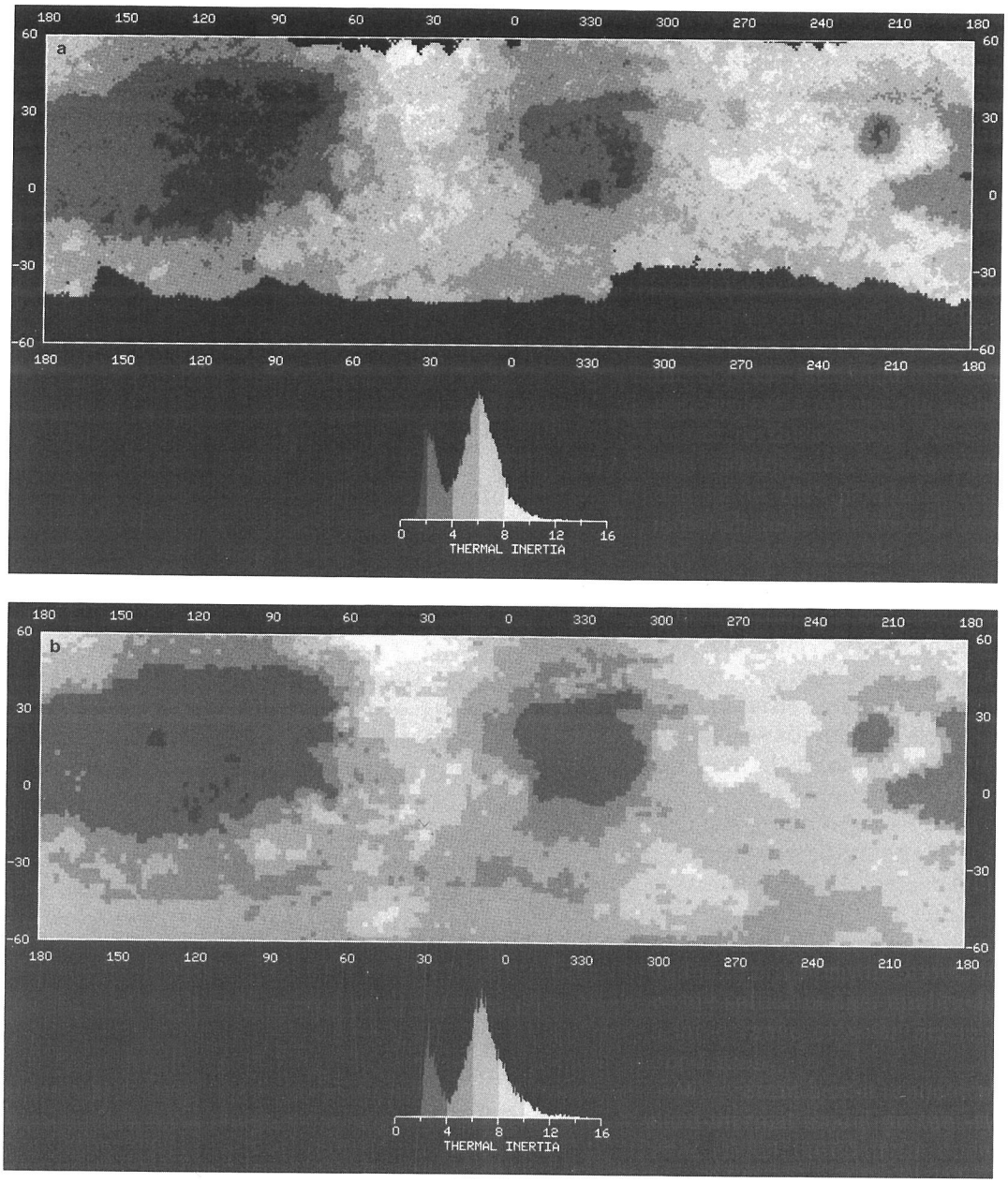

FIG. 6. Thermal inertia. (a) Fine-component thermal inertia. Values of thermal inertia were derived from the same data used to determine rock abundance shown in Fig. 5. (b) Effective thermal inertia of the composite surface (data from Palluconi and Kieffer, 1981).

urnal T_{20} observations (Palluconi and Kieffer, 1981) is also shown in Fig. 6. Removing the contribution due to high-inertia rocks lowers the inertia of the fines relative to the composite surface by about 1 but does not alter the general pattern of inertia variations observed. This similarity can be seen in a comparison of the histograms of thermal inertia (Fig. 7) where it is apparent that the bimodal character has not been altered.

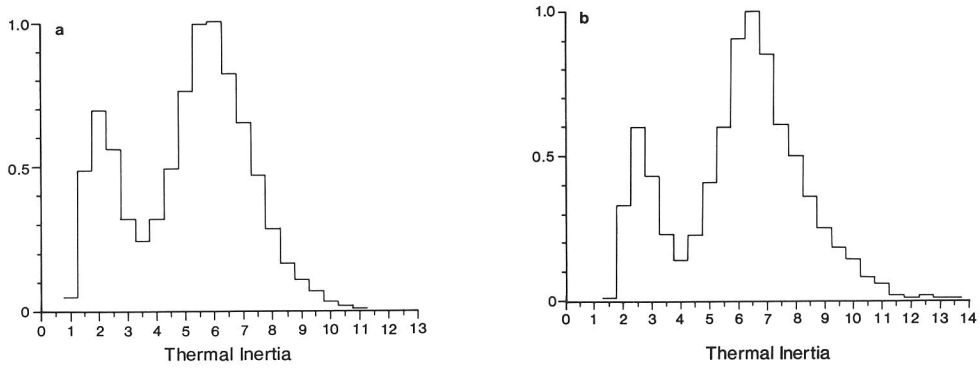

FIG. 7. Histograms of thermal inertia. (a) Fine-component inertia; (b) effective thermal inertia of the composite surface.

These global inertia values confirm previous studies which suggested that the thermal inertia is controlled primarily by the properties of the fine component, rather than by a variation in surface rocks (Christensen, 1982). Thus, low-inertia surfaces appear to be covered by fine (<40 μm sized) particles (Kieffer *et al.*, 1977), whereas high-inertia surfaces have a coarse "soil" component. In most regions this increase in apparent particle size appears to be due to variations in the degree of bonding of the surface material (Jakosky and Christensen, 1986a), whereas in some areas it is due to a real increase in grain diameter.

IV. DISCUSSION

Comparison with Global Properties

Comparison of multiple data sets for Mars has previously provided a great deal of insight into the nature of the surface (McCord *et al.*, 1982; Arvidson *et al.*, 1982; Schaber, 1980; Jakosky and Muhleman, 1981; Jakosky and Christensen, 1986a,b). These comparisons serve to illustrate the dependent and independent surface properties and provide better constraints on properties and processes acting on the surface. Several such comparisons of rock abundance with other relevant data sets are presented in the following sections.

Thermal Inertia

A comparison of the rock abundances and fine-component inertias determined here is given in Fig. 8a. Despite the observation that rocks do not control the thermal inertia of the surface, there is a weak correlation between rocks and inertia, with low-inertia surfaces having fewer rocks. This correlation is most apparent in the comparison of the population of points at low inertia, which have very few rock abundances greater than 10%, and the high-inertia points, which have a much wider range of rock abundance and values over 20%. The low-inertia regions may have undergone increased mantling by fine dust, thereby lowering the surface inertia and at the same time burying most of the exposed rocks (Christensen, 1986). Similarly, the rockiest surfaces have less dust mantling, with coarse or bonded material exposed on the surface.

Albedo

The correlation of rock abundance with the bolometric bond albedo determined from the Viking IRTM observations (Pleskot and Miner, 1981) is shown in Fig. 8b. These data are again correlated, with dark regions having more rocks than bright regions. This correlation is not surprising, however, given the previously observed

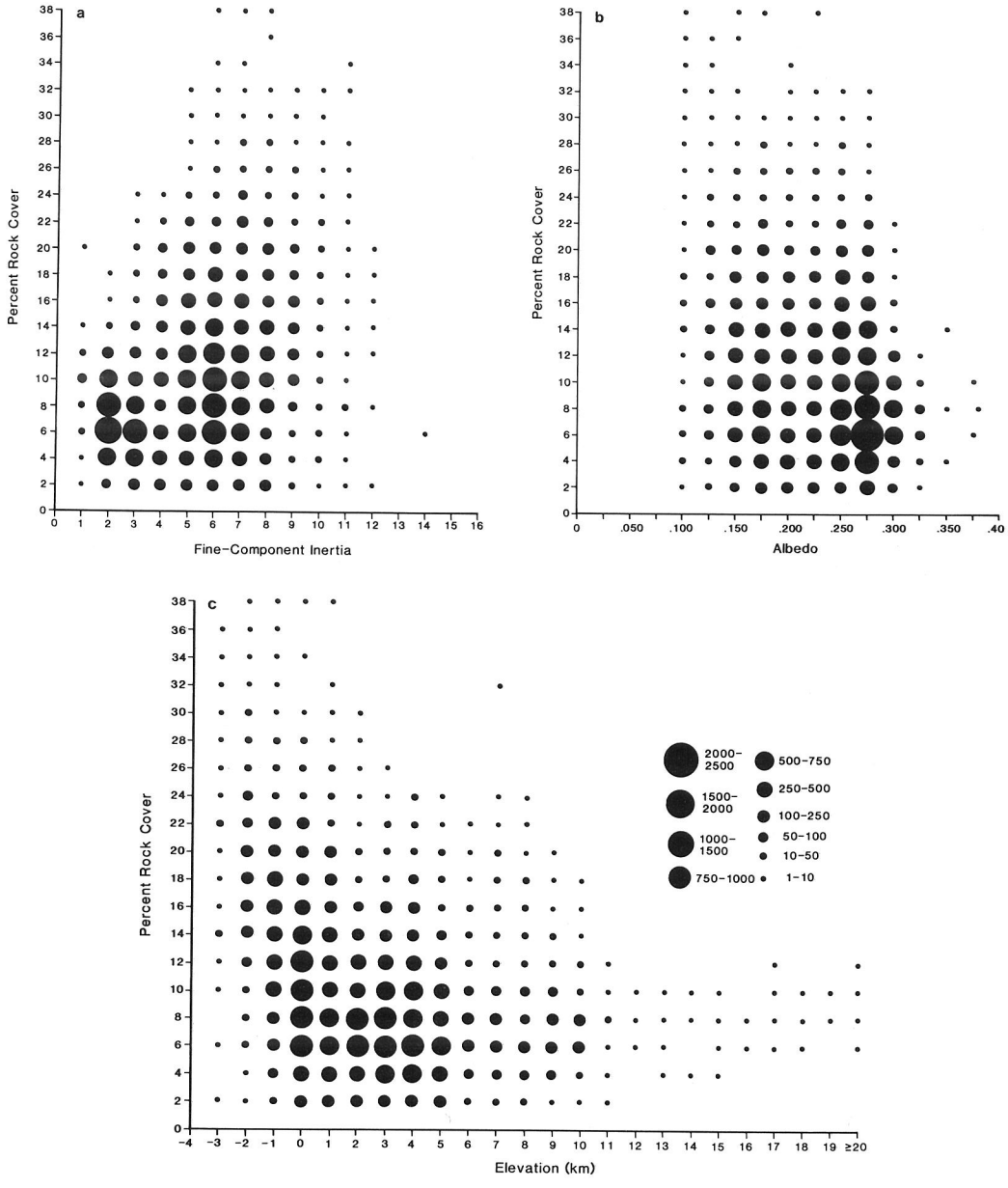

FIG. 8. Global correlation of rock abundance with surface properties. (a) Fine-component thermal inertia. (b) Albedo. Albedo data are from Pleskot and Miner, 1981. (c) Elevation. Elevation data are from U.S. Geological Survey (1976).

correlation between thermal inertia and albedo (Palluconi and Kieffer, 1981), and the correlation between rocks and inertia discussed above. It is, however, consistent with the model of increased rock abundance in the regions least mantled by fine, bright dust. The rock abundance measurements indicate that the dark regions have the least dust mantle of any regions on Mars, and may have a large amount of

rocks and rock fragments exposed at the surface, thus providing the best sites for studying the primary rock composition.

Elevation

The correlation of rock abundance with elevation is shown in Fig. 8c. There is a trend of increasing rock fraction with decreasing elevations, with the basins and other low regions on Mars having more rocks than found elsewhere. This observation is again consistent with the correlations between rocks and inertia, and inertia and elevation (Jakosky, 1979; Palluconi and Kieffer, 1981). It is important to note, however, because it provides strong evidence that the low elevation regions on Mars are not regions of sediment accumulation. Apparently, sedimentation does not occur on Mars primarily by downslope movement of material. Instead, deposition of material may be related to dust storm activity, with dust being uniformly deposited and subsequently reworked (Christensen, 1986). In this process, the deposition of fines is controlled by atmospheric and surface conditions that favor removal from regions of high surface winds, convergent atmospheric circulation, and high surface roughness (Christensen, 1986). These conditions are most likely to be found in low-lying, high-inertia regions, resulting in the observations of more exposed rocks at lower elevations.

Comparison to Radar Observations

Perhaps the most potentially instructive comparison is that between rock abundance and radar properties. The characteristics of the radar return are controlled both by dielectric constant and the surface scattering properties, which are in turn controlled in part by the distribution of surface rocks. A direct comparison of radar return "roughness" and rock abundance is complicated, however, by the sensitivity of the radar reflectivity to surface slopes, subsurface rocks, and the size and shape of the radar scatterers present, as well as to the radar technique employed (Jakosky and Christensen, 1985). Radar properties have been determined using delay-Doppler (Downs *et al.*, 1973, 1975), single-polarization continuous-wave (CW) (Simpson *et al.*, 1978a,b, 1982, and others), dual-polarization CW (Harmon *et al.*, 1982; Harmon and Ostro, 1985), and bistatic (Simpson *et al.*, 1984) observations. Each of these techniques measure somewhat different properties and provide different comparisons.

The delay-Dopper technique allows the properties of a single spatial bin to be determined, but is much more sensitive to specular reflection from the inter-rock ("soil") component than to diffuse reflection from the rocks themselves. This sensitivity occurs because the incident beam is scattered by rocks into a full hemisphere, whereas return energy is only collected from a cone within roughly 10° of the surface normal (Downs *et al.*, 1973, 1975; Jakosky and Christensen, 1985). Thus, the fraction of the scattered energy observed is small, and the signal is dominated by specular reflection from the undulating, inter-rock surface. The single-polarization CW data are sensitive to both specular reflection from the "soil" surface and to diffuse reflection from the rocks because energy is collected from a north–south strip extending to the poles. Near the sub-Earth point, specular reflection dominates, as in the delay-Doppler technique, but at the limb the diffuse component dominates. Thus, these data provide some measure, albeit not a uniquely interpretable one, of surface rockiness. Dual-polarization CW observations provide a significant improvement over single-polarization measurements because they do permit the specular and diffuse components to be separated. This separation is possible because the depolarized component contains only energy that has been diffusely reflected, whereas the polarized component contains both specular and diffuse components (Harmon *et al.*, 1982; Harmon and Ostro, 1985). Unfortunately these data exist only for a limited region of

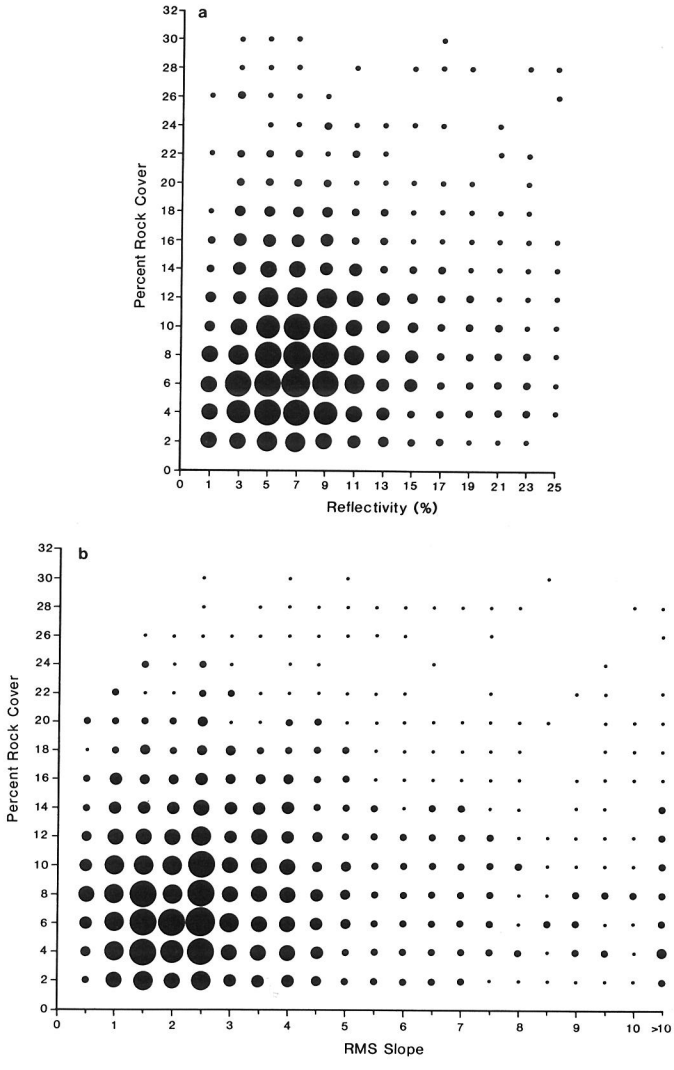

FIG. 9. Comparison of delay-Doppler radar observations and rock abundance. Radar data are from Downs *et al.*, 1975. (a) Comparison to radar reflectivity; (b) comparison to dervied RMS slope.

Mars. Finally, bistatic data produced using the Viking Orbiters also provide a measure of surface roughness by observing the specular reflection of the radar beam in the forward direction (Simpson and Tyler, 1981). However, equatorial observations are limited in extent (Simpson *et al.*, 1984).

Despite these limitations, several interesting comparisons can be made. First the rock abundance can be compared to the RMS slope and reflectivity values derived from delay-Doppler observations as shown in Fig. 9. RMS slope is a measure of the distribution of surface slopes with scale larger than a wavelength (Hagfors, 1964; Muhleman, 1964). The radar data presented in Fig. 9 were acquired during the 1971–1973 oppositions (Downs *et al.*, 1975) and cover only the southern hemisphere between −22.4°S and −14.3°S. The radar return measured is due to the "quasi-specular" component and can be produced by

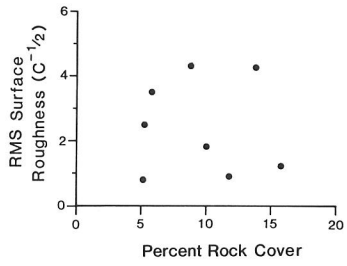

FIG. 10. Comparison of Viking bistatic radar data with rock abundance. Radar data are from Simpson *et al.*, 1984.

any combination of properly oriented surface slopes or rock facets, provided they are greater than a wavelength in size. Because the radar incidence angle is restricted to ±5°, these data are primarily sensitive to the inter-rock surfaces, with less contribution by scattering due to rocks. The radar data shown in Fig. 9 were obtained using 12.6-cm Goldstone radar, and are therefore most sensitive to 12 cm and larger facets. The individual radar resolution cells were 2° × 0.16° in latitude and longitude, and were rebinned at 2° × 2° for comparison to the rock abundance measurements.

There is little correlation between rocks and total reflectivity, with any given value of rock abundance having nearly the entire range of reflectivities observed. Similarly, there is essentially no correlation between rocks and RMS slope (Fig. 9b). These results suggest that these data sets measure different surface properties, with the delay-Doppler data being more sensitive to the inter-rock surfaces and primarily measuring variations in surface undulations and large-scale surface slopes.

Viking bistatic observations of a limited number of equatorial regions agree well with delay-Doppler measurements where they overlap (Simpson *et al.*, 1984), but do not correlate with rock abundance, as shown in Fig. 10. This lack of correlation is consistent with the lack of correlation between rock abundance and delay-Doppler roughness discussed above. Again, the bistatic results do not appear to be measuring rock abundance, but instead measure larger scale surface slopes and undulations.

There is a correlation between RMS slope determined using CW observations and rock abundance, as shown in Fig. 11. The strength and significance of this correlation is uncertain, however. Using all of the points in Fig. 11, the correlation coefficient is only 0.36. Excluding the two extreme points in this figure gives a correlation coefficient of 0.88. If these points are ignored, then there does appear to be a consistent trend of increasing RMS slope with increasing rock abundance, suggesting that the RMS slopes derived from this technique are sensitive to scattering by rocks. It must be remembered, however, that the surface covered by the radar observations extends from the sub-Earth point to the poles. One possible explanation for the agreement between rock abundance and CW measurements is the larger radar incidence angle over which the measurements were made. Increasing the angle increases the sensitivity to energy scattered into the return beam by rocks further from the sub-Earth point. The correlation may also be in part due to a correlated occurrence of rockier and more undulating surfaces in some locations.

The final radar data set that will be discussed is the dual-polarization CW results

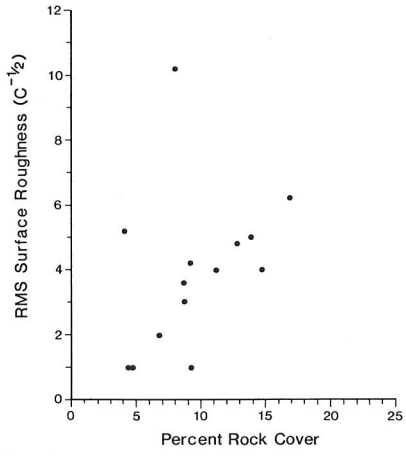

FIG. 11. Comparison of single-polarization CW radar data with rock abundance.

obtained at Arecibo Observatory in 1980 and 1982 (Harmon *et al.*, 1982, Harmon and Ostro, 1985). These measurements have only been reported for a limited region of Mars, extending around the planet at 22–24°N. These observations are sufficient, however, to demonstrate significant variability in near-surface roughness (Harmon and Ostro, 1985). The roughness derived from these data does not, however, correlate well with the thermal observations of surface rocks. In particular, the volcanic regions were found to be very efficient scatterers, indicating high coverage by decimeter-scale rocks (Harmon and Ostro, 1985). As seen in Fig. 5, however, these areas have among the lowest rock abundances observed.

One plausible explanation for this apparent contradiction is the burial of many rocks by a relatively thin (~1 m) mantle of fine dust (Christensen, 1986). This model could explain both data sets, with the radar sampling both surface and buried rocks, whereas the thermal measurements are only sensitive to the rocks exposed at the surface. Additional support for this model comes from the presence of low-inertia, bright material on the surface of these regions (Fig. 6), consistent with a mantling of fine, bright dust. The attenuation of the radar signal through a dust layer is controlled by the dielectric constant and loss tangent. The depth to which 12-cm radar could penetrate a dry, powdered material before being attenuated by a factor of $1/e$ is 60 cm to 6 m (Campbell and Ulrichs, 1969). Thus, the radar energy could penetrate a 1-m-thick dust deposit, be reflected, and exit the surface with a significant fraction of the energy that would have been reflected from an unmantled surface.

As pointed out by Harmon and Ostro (1985), the volcanic terrains would be expected to initially have been very rough, rocky surfaces. This surface morphology is not consistent, however, with the thermal inertia nor with rock abundances derived from the thermal data. It therefore appears that the present surface of these terrains has been modified by the deposition of a thin layer of dust, and that the surface exposed today is relatively smooth. Together, the thermal and radar observations place strong constraints on the thickness, and therefore the rate of deposition and age, of these deposits, and suggest active processes of dust deposition and removal.

Regional Studies

As discussed above, there are several large-scale correlations between rock abundance and morphology. Most notable are the low rock abundances observed for the Tharsis and Elysium volcanic regions, and the cratered uplands of Arabia, and the high rock abundances seen in the Coprates canyon system and in the large plain of Acidalia Planitia, into which many channels have flowed (Fig. 5). In addition to this gross character, there are numerous correlations at smaller scales, several of which will be discussed below. To aid these comparisons, the data from Fig. 5 have been separated into three rock abundance levels: 1 to 7%, 8 to 14%, and >14%. These data have been superimposed on a digital version of the 1 : 15 M shaded relief map of Mars (U.S. Geological Survey, 1982a,b), shown in Fig. 12.

Tharsis-Elysium

A low-inertia material covers the Tharsis upland, extending eastward to Lunae Planum (80°W) in the region north of Valles Marineris, and covering Amazonis Planitia to the west (Fig. 12). This entire region has relatively uniform, low (<10%) rock abundance. There are several areas, however, that have slightly higher rock abundances. One of these areas includes the Pavonis and Arsia volcanoes. These surfaces have relatively fresh appearing lava flows, with crater counts suggesting ages of 100 to 500 million years (Zimbelman, 1984). Regional geologic mapping indicates that these surfaces are slightly younger than the surrounding volcanic plains units (Zimbelman,

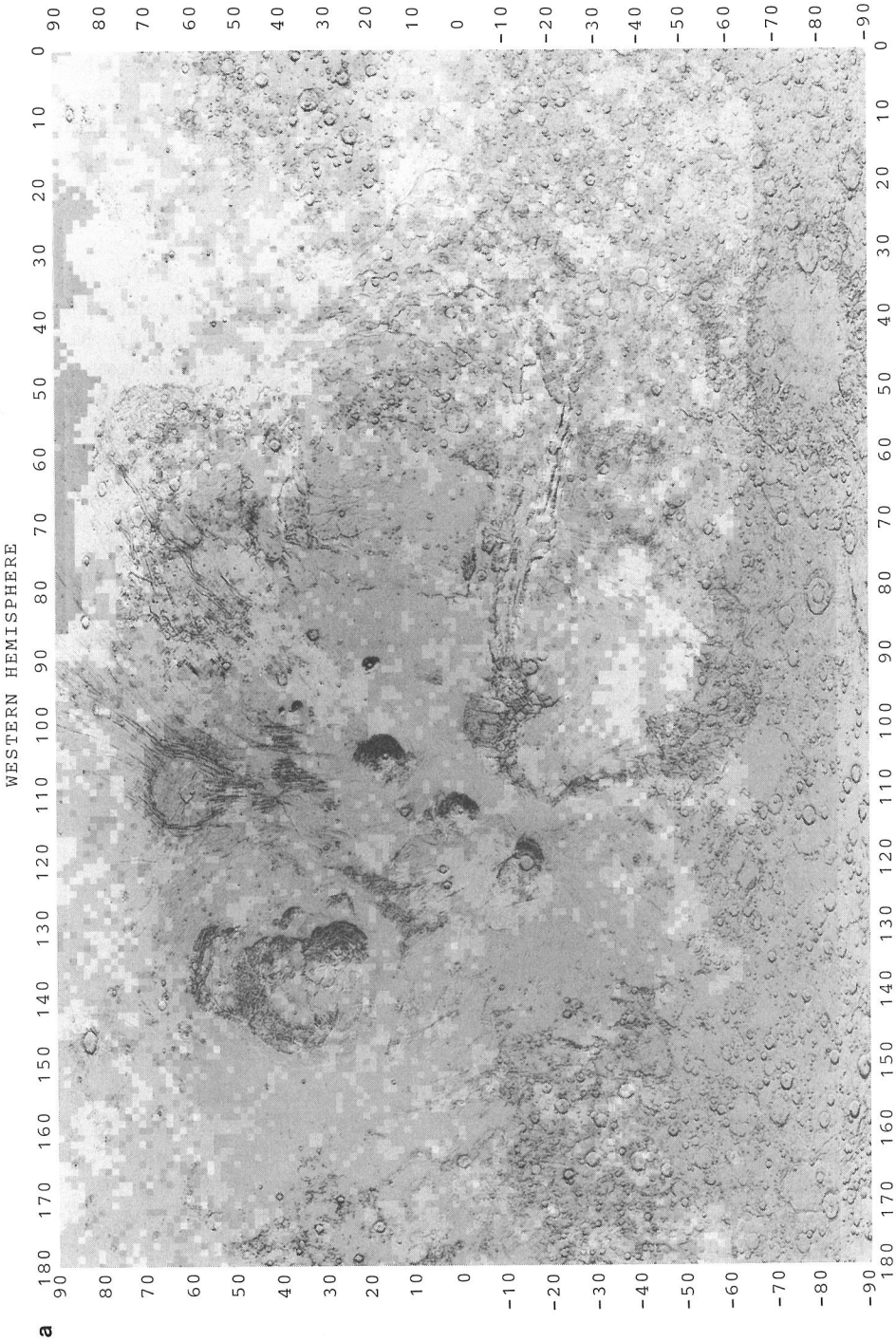
a
WESTERN HEMISPHERE
180 170 160 150 140 130 120 110 100 90 80 70 60 50 40 30 20 10 0
90 80 70 60 50 40 30 20 10 0 -10 -20 -30 -40 -50 -60 -70 -80 -90

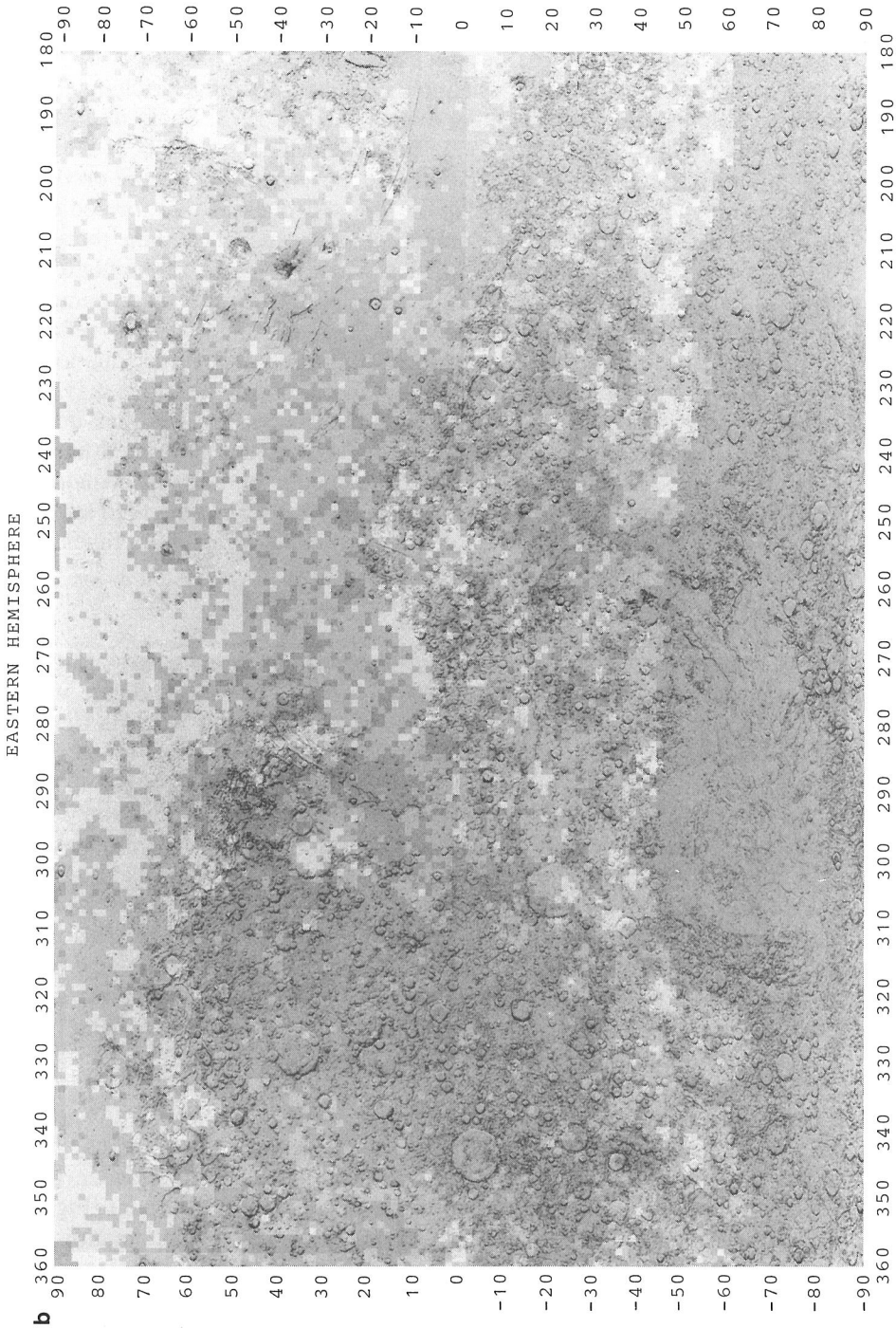

FIG. 12. Overlay of rock abundance on 1:15 M shaded relief image of Mars. Rock data are from Fig. 5, separated into three levels: 1–7%, 8–14%, and >14% rock cover. Shaded relief image is from U.S. Geological Survey (1982a,b).

1984; Scott and Tanaka, 1981), consistent with a slightly less degraded or mantled surface. It should be emphasized, however, that none of these surfaces appear to be fresh or unaltered. Parts of Olympus Mons also have a slightly higher rock abundance than the surroundings, although this pattern is not conclusive. Finally, there is a region of higher rock abundance extending along the crest of the Tharsis upland to the northeast and into the Tempe and Mareotis Fossae region.

The Elysium volcanic region also has low inertia and rock abundance. By analogy to Tharsis, much of this area may also be covered by a relatively thin (~1 m) mantle of fine, bright dust, particularly on Elysium Mons. Hecates and Albor Tholis have higher rock abundances, possibly due to less extensive mantling.

Valles Marineris Channel System

This channel system as a whole, including Ares, Tiu, and Simud Valles, displays relatively high rock abundances (Fig. 12). Much of the channel systems are at or below the spatial resolution of the rock data, making it impossible to determine variations in rock abundance along the lengths of individual channels. Numerous regions of chaotic terrain have high rock abundances, such as the region at 0 to 10°S, 25 to 30°W. In addition, regions with numerous small channels, such as the zone extending southwest from −10°S, 20°W to −30°S, 50°W, also have numerous exposed rocks.

Within Acidalia Planitia, the highest rock abundances occur around margins. In several locations, the surface is rockier where major channels widen and flow into the basin, for example, at the terminus of Ares, Simud, and Kasei Valles. Rock abundance decreases with distance into the basin from the channels. One possible explanation for this pattern may be due to the deposition of a major portion of the rocks where the flow slowed and its carrying capacity decreased. The overall high inertia of this basin is consistent with the deposition of smaller, sand-to-gravel sized particles over a much broader extent, but with the rock component concentrated near the margins.

These results are consistent with these surfaces having been produced by catastrophic collapse, flooding, or channel-cutting events (Sharp, 1973; Sharp and Malin, 1975; Baker and Kochel, 1979). If the rock abundances observed today were produced by the original processes that formed these channels and depressions, then there has been very little net dust accumulation or surface degradation in the intervening period. This lack of mantling may reflect a true lack of surface deposition, due in part to the fact that these depressions may have influenced the processes of aeolian deposition and deflations, and prevented fine material from accumulation. Alternatively, this region may have been mantled and subsequently exhumed one or more times in its history.

Antoniadi

Antoniadi crater (centered at 22°N, 299°W) has a high rock abundance within the crater rim. This occurrence is the best example of rock abundance associated with surface morphology found. There is not a close correlation between fine-component inertia and crater morphology, although the crater does lie close to a regional boundary between low- and high-inertia surfaces (Fig. 6). The cause of the observed correlation is not clear at present, but may be associated with processes operating within the crater, such as flooding of the floor by lavas.

Arabia

The Arabia region, like Tharsis, has a very uniform, low rock abundance and a bright low-inertia fine component (Fig. 12). These findings again suggest mantling by dust storm fallout. In Arabia this mantle may be thicker than in Tharsis, as indicated by the presence of subdued morphology and lowered crater abundances (Zimbelman and Kieffer, 1979; Zimbelman and Greeley,

1982) and from the lack of coarse, aeolian deposits found elsewhere (Christensen, 1983). The northern boundary of Arabia grades into a rockier surface near the border between the cratered uplands and northern plains units (Scott and Carr, 1978). However, as is found for the thermal inertia boundary (Kieffer et al., 1977; Zimbelman and Kieffer, 1979), there is not a one-to-one correlation between rock abundance and geologic unit. One explanation for the gradational boundary may be that the distribution of rocks is controlled more by the degree of mantling by dust fallout than by the underlying geology. Thus, the distribution of surface rocks may reflect a thinning of the dust mantle away from the center of Arabia.

Syrtis Major

Syrtis Major differs significantly from much of the rest of Mars, for it is a dark, moderate-inertia region that has relatively low rock abundances (Fig. 12). Earth-based radar observations indicate that the surface of Syrtis Major is very smooth in the region from 290 to 300°W, 0 to 15°N (Simpson *et al.*, 1982). As seen in Fig. 12, this region corresponds to an area of low rock abundance. This smooth surface was initially interpreted to be due primarily to resurfacing by low-viscosity lavas (Simpson *et al.*, 1982). A more plausible explanation for the smooth surface may be the presence of substantial sand deposits (Lee, 1986, submitted for publication). Dark dunes are observed in high-resolution Viking frames between 0 and 10°N and 290 to 295°W (Peterfreund, 1981), and sand may be pervasive over the entire low-albedo surface of Syrtis Major (Lee, 1986, submitted for publication). A mantle of dark sand would account for all of the remoted-sensing observations, namely: (1) the observed low rock abundance; (2) a thermal inertia consistent with sand-sized particles (Kieffer, 1973); (3) the low albedo, suggestive of a dust-free surface as could be maintained by active saltation; and (4) the smooth surface observed by radar. Therefore in Syrtis Major, as in Tharis and elsewhere, it appears that aeolian resurfacing, rather than the underlying geology, controls the distribution of surface rocks.

Solis Planum

The Solis Planum region (−20 to −30°S, 80 to 100°W) has significantly higher rock abundance than the surrounding terrain. This region contains the Solis Planum albedo feature, which is observed to vary in brightness on a seasonal and yearly basis (Lee, 1986, submitted for publication), and is also the source of local dust storms (Slipher, 1962; Martin, 1976). This area has been interpreted as a region of intense aeolian activity, with substantial erosion of fine material (Lee, 1986, submitted for publication). One consequence of this activity may be the production of a significant number of surface rocks, as is observed. In this case, Solis Planum may represent an area on Mars that is currently undergoing active erosion, in contrast to the northern-hemisphere low-inertia deposits which have been proposed to be undergoing active deposition (Christensen, 1986). This observation is consistent with a general south-to-north transport of fine material.

IV. CONCLUSIONS

Using the distribution of surface rocks derived from thermal observations, a number of conclusions can be reached regarding the surface properties and processes of Mars. Rocks appear to be ubiquitous on the surface, with no regions of the size sampled (1° × 1°) being rock free. The modal value of rock abundance is 6%, and there are no regions that have more than 30–35% areal rock cover. Once the rock contribution is removed, it is found that the thermal inertia of the fine component, rather than the abundance of rocks, produces the observed variation in bulk thermal inertia. This result implies a real variation in fines over the planet, either due to variations in degree of bonding or particle size. In general, the

rock abundances do not correlate well with RMS surface roughness as determined by delay-Doppler or bistatic radar measurements, but do show a possible correlation with roughness derived from continuous-wave, single-polarization radar measurements. These observations suggest that the roughness determined from most radar observations is only weakly dependent on the distribution of small-scale rocks. Dual-polarization radar data can be used to separate rocks and slopes and, in the Tharsis region, indicate that the surface is very rough. In contrast, the rock abundance derived from thermal data is relatively low. This inconsistency may be due to partial burying of rocks by dust, with the radar sampling subsurface rocks, whereas the thermal data only sample the less abundant rocks that are exposed on the surface.

Most bright, low-inertia surfaces have few rocks, whereas dark, high-inertia surfaces are relatively rocky. This correlation is consistent with mantling of rocks and coarse material by bright dust. Regional studies reveal that the Valles Marineris system, Ares, Tiu, Simud, and other flood channels, and several regions of chaotic terrain, all have relatively high rock abundances. In addition, the Acidalia Planitia basin has a high rock abundance, with some indication of rockier surfaces near the margins of the basin and at the terminus of channels. This rock distribution may be due to the deposition of the coarsest fraction of the load carried by the flood near where the flow entered the basin. If a relic of the initial surface, it would imply little modification in the intervening period. Syrtis Major is a very dark region that has few rocks. The observed presence of dunes suggests that this region is also mantled by aeolian material, but in this case by coarse, mobile sand rather than dust. The global distribution of rocks indicates that resurfacing by aeolian material, rather than the initial generation of rocks, controls the distribution observed at the present time.

ACKNOWLEDGMENTS

I would like to thank Mike Malin, Rich Zurek, Steve Lee, and Ronald Greeley for many fruitful discussions during the course of this work. I especially wish to thank Bruce Jakosky for many helpful comments, particularly regarding the interpretation of the radar data. Peter Thomas and Bruce Jakosky provided thorough reviews which improved the manuscript. All images were processed using the Arizona State University Image Processing Facility.

REFERENCES

Arvidson, R. E., E. A. Guinness, and A. P. Zent (1982). Classification of surface units in the equatorial region of Mars based on Viking Orbiter color, albedo, and thermal data. *J. Geophys. Res.* **87,** 10,149–10,157.

Baker, V. R., and R. C. Kochel (1979). Martian channel morphology: Maja and Kasei Valles. *J. Geophys. Res.* **84,** 7961–7983.

Binder, A. B., R. E. Arvidson, E. A. Guinness, K. L. Jones, E. C. Morris, T. A. Mutch, D. C. Pieri, and C. Sagan (1977). The geology of the Viking Lander 1 site. *J. Geophys. Res.* **82,** 4439–4451.

Campbell, M. J., and J. Ulrichs (1969). Electrical properties of rocks and their significance for lunar radar observations. *J. Geophys. Res.* **74,** 5867–5881.

Christensen, P. R. (1982). Martian dust mantling and surface composition: Interpretation of thermophysical properties. *J. Geophys. Res.* **87,** 9985–9998.

Christensen, P. R. (1983). Eolian intracrater deposits on Mars: Physical properties and global distribution. *Icarus* **56,** 496–518.

Christensen, P. R. (1984). Thermal emissivity of the Martian surface: Evidence for compositional variations. *Lunar Planet Sci.* **XV,** 150–151.

Christensen, P. R. (1986). Regional dust deposits on Mars: Physical properties, age, and history. *J. Geophys. Res.* **91,** 3533–3546.

Christensen, P. R., and R. W. Zurek (1984). Martian north polar hazes and surface ice: Results from the Viking Survey/Completion mission. *J. Geophys. Res.* **89,** 4587–4596.

Christensen, P. R., R. W. Zurek, and L. L. Jaramillo (1986). Seasonal and diurnal variability of Mars water-ice clouds. *Lunar Planet Sci.* **XVII,** 123–124.

Conrath, B., R. Curran, R. Hanel, V. Kunde, W. Maguire, J. Pearl, J. Pirraglia, and J. Welker (1973). Atmospheric and surface properties of Mars obtained by infrared spectroscopy on Mariner 9. *J. Geophys. Res.* **78,** 4267–4278.

Cuzzi, J. N., and D. O. Muhleman (1972). The microwave spectrum and the nature of the subsurface of Mars. *Icarus* **17,** 548–560.

DOWNS, G. S., R. M. GOLDSTEIN, R. R. GREEN, G. A. MORRIS, AND P. E. REICHLEY (1973). Martian topography and surface properties as seen by radar: The 1971 opposition. *Icarus* **18,** 8–21.

DOWNS, G. S., P. E. REICHLEY, AND R. R. GREEN (1975). Radar measurements of Martian topography and surface properties: The 1971 and 1973 oppositions. *Icarus* **26,** 273–312.

HAGFORS, T. (1964). Backscattering from an undulating surface with applications to radar returns from the Moon. *J. Geophys. Res.* **69,** 3779–3784.

HARMON, J. K., D. B. CAMPBELL, AND S. J. OSTRO (1982). Dual-polarization radar observations of Mars: Tharsis and environs. *Icarus* **52,** 171–187.

HARMON, J. K., AND S. J. OSTRO (1985). Mars: Dual-polarization radar observations with extended coverage. *Icarus* **62,** 110–128.

JAKOSKY, B. M. (1979). The effects of non-ideal surfaces on the derived thermal properties of Mars. *J. Geophys. Res.* **84,** 8252–8262.

JAKOSKY, B. M. (1986). On the thermal properties of martian fines. *Icarus* **66,** 117–124.

JAKOSKY, B. M., AND D. O. MUHLEMAN (1980). The longitudinal variation of the thermal inertia and of the 2.8 cm brightness temperature of Mars. *Astrophys. J.* **239,** 403–409.

JAKOSKY, B. M., AND D. O. MUHLEMAN (1981). A comparison of the thermal and radar characteristics of Mars. *Icarus* **45,** 25–28.

JAKOSKY, B. M., AND P. R. CHRISTENSEN (1985). Interpretation of remote sensing observations of Mars. *Lunar Planet. Sci.* **XVI,** 392–393.

JAKOSKY, B. M., AND P. R. CHRISTENSEN (1986a). Global duricrust on Mars: Analysis of remote sensing data. *J. Geophys. Res.* **91,** 3547–3560.

JAKOSKY, B. M., AND P. R. CHRISTENSEN (1986b). Are the Viking Lander sites representative of the surface of Mars? *Icarus* **66,** 125–133.

KIEFFER, H. H., S. C. CHASE, JR., E. MINER, G. MUNCH, AND G. NEUGEBAUER (1973). Preliminary report on infrared radiometric measurements from Mariner 9 spacecraft. *J. Geophys. Res.* **78,** 4291–4312.

KIEFFER, H. H., T. Z. MARTIN, A. R. PETERFREUND, B. M. JAKOSKY, E. D. MINER, AND F. D. PALLUCONI (1977). Thermal and albedo mapping of Mars during the Viking primary mission. *J. Geophys. Res.* **82,** 4249–4292.

LEE, S. W. (1986). Seasonal and secular variation of the Solis Lacus albedo feature: Relation to the martian dust-transport cycle. Submitted to Icarus.

MARTIN, L. J. (1976). 1973 Dust Storms on Mars: Maps from Hourly Photographs. *Icarus* **29,** 363–380.

MARTIN, T. Z. (1986). Thermal infrared opacity of the Mars atmosphere. *Icarus* **66,** 2–21.

MCCORD, T. B., R. B. SINGER, B. R. HAWKE, J. B. ADAMS, D. L. EVANS, J. W. HEAD, P. J. MOUGINIS-MARK, C. M. PIETERS, R. L. HUGUENIN, AND S. H. ZISK (1982). Mars: Definition and characterization of global surface units with emphasis on composition. *J. Geophys. Res.* **87,** 10,129–10,148.

MUHLEMAN, D. O. (1964). Radar scattering from Venus and the moon. *Astron. J.* **69,** 34–41.

MUTCH, T. A., R. A. ARVIDSON, A. B. BINDER, E. A. GUINNESS, AND E. C. MORRIS (1977). The geology of the Viking Lander 2 site. *J. Geophys. Res.* **82,** 4452–4467.

PALLUCONI, F. D., AND H. H. KIEFFER (1981). Thermal inertia mapping of Mars from 60°S to 60°N. *Icarus* **45,** 415–426.

PETERFREUND, A. R. (1981). Visual and infrared observations of wind streaks on Mars. *Icarus* **45,** 447–467.

PLESKOT, L. K., AND E. D. MINER (1981). Time variability of Martian bolometric albedo. *Icarus* **45,** 179–201.

POLLACK, J. B., D. S. COLBURN, F. M. FLASAR, R. KAHN, C. E. CARLSTON, AND D. PIDEK (1979). Properties and effects of dust particles suspended in the Martian atmosphere. *J. Geophys. Res.* **84,** 2929–2945.

SCHABER, G. G. (1980). Radar, visual and thermal characteristics of Mars: Rough planar surfaces. *Icarus* **42,** 159–184.

SCOTT, D. H., AND M. H. CARR (1978). Geologic map of Mars. U.S. Geol. Surv. Misc. Invest. Ser., Map I-1083.

SCOTT, D. H., AND K. L. TANAKA (1981). Paleostratigraphic restoration of buried surfaces in Tharsis Montes. *Icarus* **45,** 304–319.

SEIFF, A., AND D. B. KIRK (1977). Structure of the atmosphere of Mars in summer at mid-latitudes. *J. Geophys. Res.* **82,** 4364–4378.

SHARP, R. P. (1973). Mars: Fretted and chaotic terrains. *J. Geophys. Res.* **78,** 4073–4083.

SHARP, R. P., AND M. C. MALIN (1975). Channels on Mars. *Geol. Soc. Amer. Bull.* **86,** 593–609.

SIMPSON, R. A., G. L. TYLER, AND D. B. CAMPBELL (1978a). Arecibo radar observations of Mars surface characteristics in the northern hemisphere. *Icarus* **36,** 153–173.

SIMPSON, R. A., G. L. TYLER, AND D. B. CAMPBELL (1978b). Arecibo radar observations of martian surface characteristics near the equator. *Icarus* **33,** 102–115.

SIMPSON, R. A., AND G. L. TYLER (1981). Viking bistatic radar experiment: Summary of first-order results emphasizing north polar data. *Icarus* **46,** 361–389.

SIMPSON, R. A., G. L. TYLER, J. K. HARMON, AND A. R. PETERFREUND (1982). Radar measurement of small scale surface texture: Syrtis Major. *Icarus* **49,** 258–283.

SIMPSON, R. A., G. L. TYLER, AND G. G. SCHABER (1984). Viking bistatic radar experiment: Summary

of results in near-equatorial regions. *J. Geophys. Res.* **89,** 10,385–10,404.

SLIPHER, E. C. (1962). *The Photographic Story of Mars*. Sky Publ. Corp., Cambridge, Mass.

THORPE, T. E. (1977). Viking Orbiter photometric observations of the Mars phase function July through November 1976. *J. Geophys. Res.* **82,** 4161–4165.

THORPE, T. E. (1982). Martian surface properties indicated by the opposition effect. *Icarus* **49,** 398–415.

TOON, O. B., J. B. POLLACK, AND C. SAGAN (1977). Physical properties of the particles comprising the Martian dust storm of 1971–1972. *Icarus* **3,** 663–696.

U.S. Geological Survey (1982a). Shaded Relief Map of the Western Region of Mars, 1 : 15,000,000 series, Map I-1320. U.S. Geological Survey, Reston, Va.

U.S. Geological Survey (1982b). Shaded Relief Map of the Western Region of Mars, 1 : 15,000,000 series, Map I-1321. U.S. Geological Survey, Reston, Va.

ZIMBELMAN, J. R. (1984). Geologic interpretations of remote sensing data for the Martian volcano Ascraeus Mons. Ph.D. thesis, Arizona State University.

ZIMBELMAN, J. R., AND H. H. KIEFFER (1979). Thermal mapping of the northern equatorial and temperature latitudes of Mars. *J. Geophys. Res.* **84,** 8239–8251.

ZIMBELMAN, J. R., AND R. GREELEY (1982). Surface properties of ancient cratered terrains in the northern hemisphere of Mars. *J. Geophys. Res.* **87,** 10,181–10,189.

ZUREK, R. W. (1982). Martian great dust storms: An update. *Icarus* **50,** 288–310.